International Core Journal of Engineering Volume 11 Issue 5, 2025
ISSN: 2414-1895 DOI: 10.6919/ICJE.202505_11(5).0001

Controllable Growth and Optical Properties of $CsPbBr_3$ Perovskite Micro/Nanostructures by Chemical Vapor Deposition

Zhengxuan Lin, Duan Zhao*, Shuai Sun, Xiaofang Lai, Shibin Lei, Jikang Jian

School of Physics and Optoelectronic Engineering, Guangdong University of Technology, Guangzhou, Guangdong, 510006, China

Abstract

In this study, perovskite structures with diverse morphologies, including microplates, microdisks and nanowires, were synthesized via chemical vapor deposition. The effects of precursor grinding treatment, precursor quantity, substrate position and reaction temperature on the morphology and dimensions of products were systematically investigated. It demonstrates that when CsBr and $PbBr_2$ powders were placed in separate crucibles without grinding, microplates with lateral a size of 30 – 60 μm, sharp edges and smooth surfaces were obtained. The size of the microplates increased if the substrate was closer to the precursor source. In contrast, when CsBr and $PbBr_2$ powders were thoroughly mixed and ground before reaction, the resulting microplates were smaller in size. By adjusting the precursor quantity and grinding treatment, the lateral size and thickness of the microplates could be controlled. By reducing the precursor quantity and placing the substrate farther away from the precursor source, circular microdisks with a plano-convex lens-like morphology were obtained. The microdisks exhibited smooth surfaces, with thickness decreasing gradually from center to edge. They displayed colorful Newton's ring interference patterns. When the reaction temperature was lowered, simultaneously with a further source-substrate distance, the product morphology transformed into nanowires. The photoluminescence (PL) spectra revealed emission peaks at 520 nm for the microplate, at 519 nm for the microdisk and at 515 nm for the nanowire, exhibiting typical PL peaks of CsPbBr. This study achieved the controllable synthesis of various CsPbBr perovskite micro/nanostructures and analyzed their morphology-property relationship, providing a significant theoretical and experimental foundation for the application of perovskite micro/nanostructures in optoelectronic fields.

Keywords

$CsPbBr_3$; Chemical Vapor Deposition; Microplates; Microdisks; Nanowires.

1. Introduction

In recent years, perovskite materials have shown great potential for applications in various fields due to their exceptional optoelectronic properties, such as wavelength tunability[1], low lasing thresholds[2], high spectral coherence[3], long carrier diffusion lengths[4], and high photoluminescence (PL) quantum yields[5]. These characteristics have attracted significant interest in perovskite materials for applications in solar cells[6], light-emitting diodes[7], lasers[8], photodetectors[9], and backlight displays. Cesium lead bromide ($CsPbBr_3$) perovskite has become a focus of current research due to its high chemical stability and outstanding PL performance. Researchers have successfully synthesized $CsPbBr_3$ perovskite materials with diverse morphologies through various methods, ranging from zero-dimensional structures (e.g. quantum dots) to one-dimensional structures (e.g. nanowires), two-dimensional structures (e.g. thin films, nanosheets) and

ISSN: 2414-1895 DOI: 10.6919/ICJE.202505_11(5).0001

multi-dimensional structures (e.g. nanocomposites)[10,11]. However, the controllable synthesis of perovskite micro/nanostructures with specific morphologies and dimensions, along with the tuning of their optical properties, has become a hot topic in current research.

Among various synthesis methods, chemical vapor deposition (CVD) has become a key technique for perovskite material synthesis. It can precisely control the morphology and dimensions of products by adjusting the growth parameters such as reaction temperature, precursor grinding treatment, precursor quantity and substrate position et al. CVD can modulate the material morphology over a wide range and facilitate the fabrication of high quality perovskite micro/nanostructures through optimized growth parameters[12,13]. Nevertheless, despite the notable advantages of CVD in perovskite synthesis, researches on the controllable synthesis of diverse $CsPbBr_3$ micro/nanostructures and their morphology-optical property relationship remains limited. Specifically, the optimization of growth parameters, including reaction temperature, precursor grinding treatment, precursor quantity and substrate position for micro/nanostructures with different morphologies still requires systematic exploration through extensive experimental work.

In this paper, we systematically investigated the effect of CVD growth parameters on $CsPbBr_3$ morphologies and their optical properties. The effects of reaction temperature, precursor grinding treatment, precursor quantity and substrate position on the morphology and dimensions of products were comprehensively studied. Microplates, microdisks and nanowires were obtained by adjusting the CVD growth parameters. It was demonstrated that these growth factors significantly influenced the morphology and dimensions of products. Appropriate reactant concentration and temperature gradients effectively modulated the morphology and crystallinity of the products. The microdisks exhibited the best PL performance owing to their good crystallinity and plano-convex lens-like morphology, whereas nanowires exhibited the weakest PL emission. This study offers detailed and comprehensive insights for the controllable synthesis of perovskite micro/nanostructures. Meanwhile, it provides an in-depth exploration of the relationship between morphology and properties, laying a foundation for further application of perovskite materials in optoelectronics.

2. Methods

$CsPbBr_3$ micro/nanostructures were synthesized via CVD in a tube furnace. CsBr (Aladdin, 99.9%) and $PbBr_2$ (Aladdin, 99.999%) precursors were either placed separately in two crucibles without grinding treatment, or thoroughly mixed and ground after which an appropriate amount of the ground mixture was placed in a crucible. The silicon (Si) substrates, cleaned by ultrasonication, were positioned downstream at a distance of 25 – 30 cm from the precursor source. The reaction was conducted at temperatures ranging from 550 °C to 575 °C. During the growth process, the precursors were evaporated in the central zone of the furnace, transported by Ar carrier gas, and then, deposited onto the silicon substrates forming $CsPbBr_3$ micro/nanostructures with diverse morphologies.

The morphology of the samples was characterized using scanning electron microscopy (SEM, SU8010, Hitachi), optical microscopy (OM, M70, Daoyi) and atomic force microscopy (AFM, Dimension FastScan, Bruker). The elemental analysis was characterized using energy-dispersive X-ray spectroscopy (EDS). The phase structure was analyzed by X-ray diffraction (XRD, Ultima IV, Rigaku). Additionally, the PL spectra of the samples were measured using a micro-confocal Raman spectrometer (Raman, LabRAM HR Evolution, HORIBA Jobin Yvon) with an excitation wavelength of 325 nm.

3. Results and Discussion

3.1 Synthesis of Microplates

0.050 g of CsBr and 0.086 g of $PbBr_2$ powders were placed separately in two crucibles at the center zone of furnace tube. The substrate was positioned downstream at a distance of 20 cm from the tube furnace center. The vapor deposition reaction was conducted at 575 °C for 20 minutes, yielding microplates with lateral dimensions of 30-60 μm, sharp edges and smooth surfaces, as illustrated in

ISSN: 2414-1895 DOI: 10.6919/ICJE.202505_11(5).0001

Figure 1(a). The lateral size of microplates increases slightly for substrate positions closer to the precursor. Figure 1(b) presents a typical SEM image of a microplate grown farther from the precursor source, with a side length of 31 μm, while Figure 1(c) shows a typical SEM image of a microplate grown closer to the precursor source, with a side length of about 48 μm. This phenomenon can be attributed to the higher temperature for the substrate position closer to the precursor source, which enhances the diffusion rate of reactant molecules, facilitating the migration and adsorption of reactants on the substrate surface and promoting crystal growth. Additionally, the higher precursor concentration near the source provides an abundant material supply for crystal growth, enabling more reactants to deposit and grow on the substrate. These two factors collectively contribute to the expansion of the microplates in both lateral and vertical directions, which result in increased lateral size and thickness[14].

Comparative experiments with thoroughly ground CsBr/$PbBr_2$ mixtures (0.14 g crucible loading) produced microplates exhibiting significantly reduced lateral dimensions of 2-10 μm (Figure 1(d)), contrasting sharply with the 30-60 μm microplates obtained from unground precursors. In summary, by adjusting the substrate position and the grinding treatment, the size of the microplates could be controlled in a wide range.

3.2 Synthesis of Microdisks

By reducing the precursor quantity from 0.14 g to 0.08 g and increasing the source-substrate distance to 23 cm, circular microdisks with a plano-convex lens-like structure were successfully fabricated. The microdisks exhibited smooth surfaces, with thickness decreasing gradually from center to edge. The microdisks display prominent colorful Newton's ring interference patterns under the optical microscope. The diameters of these microdisks ranged from 4 to 33 μm, as shown in Figure 1(e). The insert in Figure 1(e) shows a typical 3-dimentional AFM image of a microdisk. The brighter region exhibits the thicker region of the microdisk, while the darker region exhibits the thinner region.

3.3 Synthesis of Nanowires

Compared with the microdisk synthesis, when the reaction temperature was reduced from 575 °C to 550 °C and the source-substrate distance was further increased to 24 cm, The product transformed to nanowires with diameters of 40-150 nm and lengths of 1-17 μm, as shown in Figure 1(f).

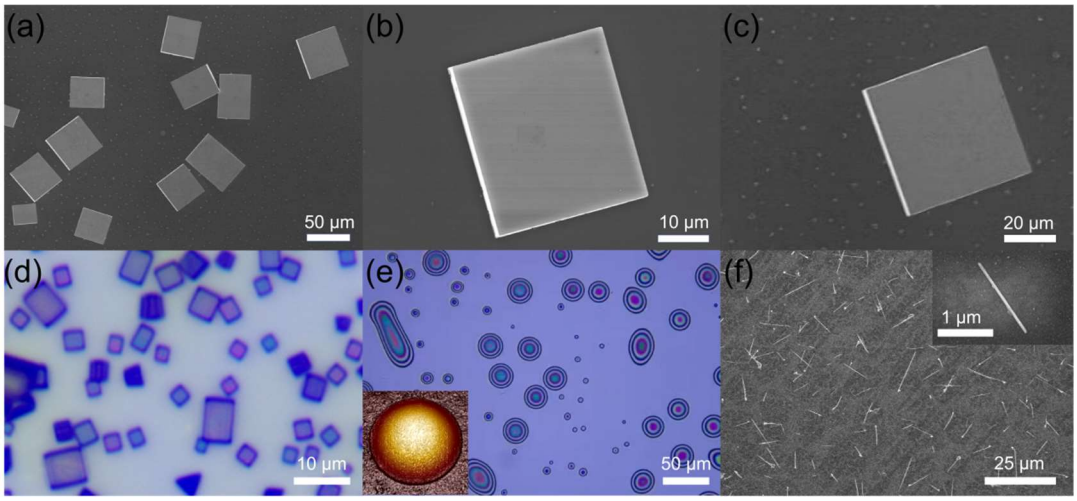

Figure 1. (a) SEM image of microplates synthesized from unmixed and unground precursors; (b) Typical SEM image of a microplate grown in the region of the substrate farther from the precursor source; (c) Typical SEM image of a microplate grown in the region of the substrate closer to the precursor source; (d) Optical microscopy image of microplates synthesized from mixed and ground precursors; (e) Optical microscopy image of plano-convex lens-like microdisks，the insert shows the 3-dimentional AFM image of a microdisk; (f) SEM image of nanowires, the insert shows the magnified SEM image of a nanowire.

ISSN: 2414-1895 DOI: 10.6919/ICJE.202505_11(5).0001

The growth conditions for microplates, microdisks and nanowires are summarized in Table 1. Microplate synthesis required elevated temperature and larger precursor quantity, both critical for sustaining high reactant concentration in the tube furnace to drive deposition, nucleation, and growth at the substrate. In contrast, microdisk synthesis utilized significantly reduced precursor quantity and greater source-substrate distance compared with microplate growth. These two factors contribute to the decreased reactant concentration and the lower temperature of the substrate. It results in the obvious decreasing reactant concentration during growth and slower growth velocity, which cannot maintain the lateral direction growth in the whole growth time and thus the lateral size decreases gradually layer by layer. Finally, plano-convex lens-like microdisks are formed. For nanowires growth, the temperature is lower and the source-substrate distance is farther compared with microdisks. These two factors contribute to the much lower reactant concentration during growth. The nucleation density is significantly decreased and sparse at the substrate, which cannot maintain the lateral growth in the initial stage and result in nanowires.

Table 1. Growth conditions for perovskite micro/nanostructures with different morphologies

Morphology	Temperature (°C)	Source-Substrate Distance(cm)	Gas Flow Rate(sccm)	Precursor Quantity(g)
Microplates	575	20	15	0.14
Microdisks	575	23	15	0.08
Nanowires	550	24	15	0.08

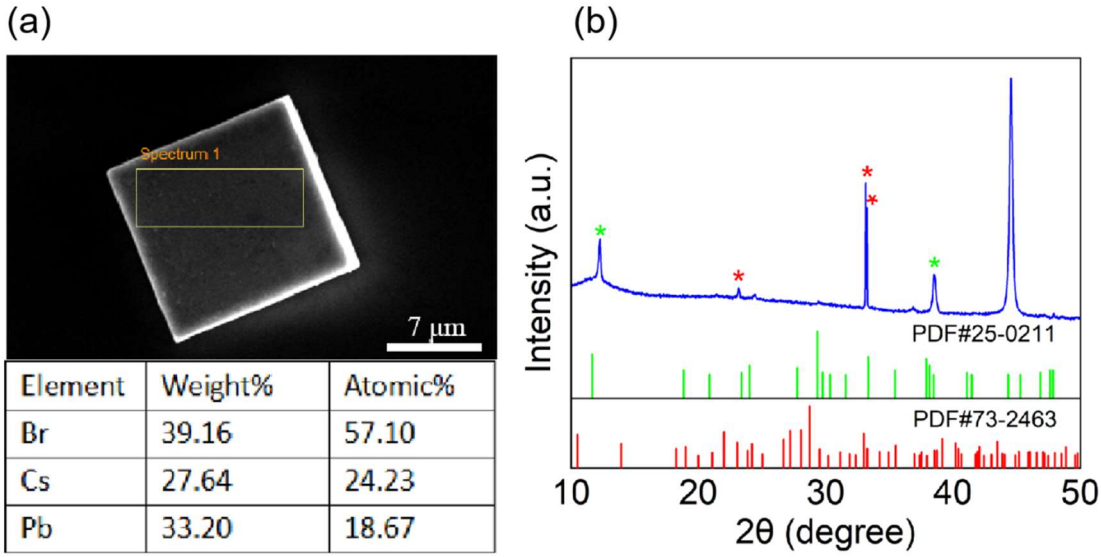

Element	Weight%	Atomic%
Br	39.16	57.10
Cs	27.64	24.23
Pb	33.20	18.67

Figure 2. (a) EDS characterization of a microplate; (b) XRD pattern of the microdisks.

As shown in Figure 2(a), the microplates were characterized using EDS for elemental analysis. The results revealed that the atomic ratio of Cs, Pb and Br was approximately 1:1:3, suggesting that the microplates are primarily composed of $CsPbBr_3$. The slightly higher Cs content may be attributed to non-uniform elemental distribution.

ISSN: 2414-1895 DOI: 10.6919/ICJE.202505_11(5).0001

The phase composition of the microdisks was analyzed using XRD, as illustrated in Figure 2(b). The narrow full-width-at-half-maximum (FWHM) and high signal-to-noise ratio of the diffraction peaks indicate excellent crystalline quality of the microdisks. The primary diffraction peaks at 23.2°, 33.1° and 33.2° correspond to the cubic phase of $CsPbBr_3$ (PDF# 73-2463). Additionally, the diffraction peaks at 12° and 38.3° are consistent with the tetragonal phase of $CsPb_2Br_5$ (PDF# 25-0211). The peak at 44.5° is attributed to the metal sample holder. The results indicate that the sample is a mixture of $CsPbBr_3$ and $CsPb_2Br_5$. Notably, the XRD diffraction peaks of the sample exhibit a slight rightward shift compared with the standard reference of $CsPb_2Br_5$ (PDF# 25-0211). This shift might be attributed to the thickness difference between the groove structure of the XRD sample holder and the **plano-convex lens-like** microdisks on the silicon substrate[15,16].

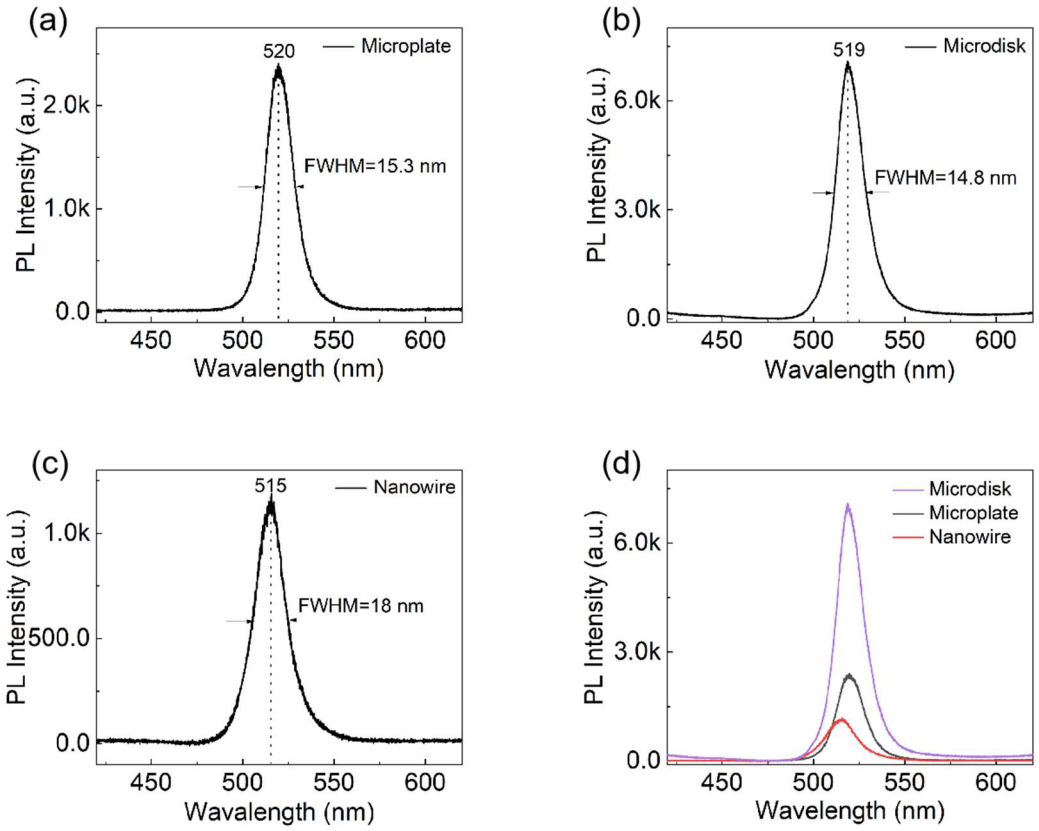

Figure 3. (a)-(c) PL spectra of a microplate, microdisk and nanowire, respectively. (d) Comparision of PL spectra for three different samples.

The PL spectra of different perovskite micro/nanostructures are presented in Figure 3. Figure 3(a)-(c) show the typical PL spectra of a microlate, microdisk and nanowire. The emission peaks of the microplate and microdisk are located at 520 nm and 519 nm, while that of the nanowire is observed at 515 nm, all corresponding to the characteristic PL emission of $CsPbBr_3$.The FWHMs for the microplate, microdisk and nanowire PL emission are 15.3 nm, 14.8 nm and 18.0 nm, respectively. A blueshift in the PL peak is observed for the nanowire. This phenomenon may be attributed to the following reasons. First, the smaller diameter of the nanowires (40 – 150 nm) may result in lower heat dissipation capability compared with the microdisk and microplate. When the sample is irradiated by laser, the introduced thermal effect can lead to a higher localized temperature in nanowire than in microdisk and microplate, which contributes to the observed blueshift of PL emission for $CsPbBr_3$[17,18]. Additionally, the diameter of the nanowire is much smaller than that of the microplate and microdisk. As a result, the exciton-phonon coupling in the nanowire is likely weaker compared with that in the microplate and microdisk. The weaker exciton-phonon coupling

ISSN: 2414-1895 DOI: 10.6919/ICJE.202505_11(5).0001

may further contribute to the blueshift of PL emission[19]. As shown in Figure 3(d), the three structures exhibit a sequential decline in PL intensity. The microdisk demonstrates the strongest PL emission peak and narrowest FWHM, indicating superior photoluminescence performance, followed by the microplate, while the nanowire displays the worst PL performance. This trend arises primarily from crystallinity variation, thermal effect, and photon confinement mechanism. Nanowires, synthesized at a lower temperature, may exhibit poorer crystallinity and higher surface-to-volume ratio, increasing the likelihood of surface defects such as uncoordinated Pb^{2+} dangling bonds and Br^{-} vacancies. These surface defects can act as non-radiative recombination centers, trapping photogenerated carriers and suppressing radiative recombination, thereby reducing the luminescence intensity[20-23]. Besides, the higher local temperature under laser irradiation may also contribute to the low PL intensity for the nanowire17. On the other hand, for nanowires, the diameters are much smaller than the emission wavelength. This can cause the light scatters and escape from the nanowire more easily, reducing the efficiency of light-matter interaction and decreasing the PL emission[24]. The largest FWHM (about 18.0 nm) for the nanowire is also attributed to its poorer crystallinity, lower heat dissipation capability and worse light confinement. In contrast, the microdisks and microplates, grown at higher temperature, possess better crystallinity. Their larger size compared with the nanowire contribute to their better heat dissipation capability and light confinement[25]. The FWHMs for the microdisk (about 14.8 nm) and microplate (about 15.3 nm) are smaller than that for the nanowire. The smallest FWHM for the microdisk also indicates its best optical performance, consistent with its strongest PL emission. Meanwhile, The continuous curvature of the microdisk minimizes edge scattering and enhances light-matter interaction, synergistically improving its PL performance[26].

4. Conclusion

In this study, we successfully synthesized perovskite microplates, microdisks and nanowires via CVD. Systematic investigation of precursor grinding treatment, precursor quantity, substrate position and reaction temperature revealed their critical roles in tuning morphology and dimensions, enabling controlled growth of these distinct architectures. Among the structures, the microdisks exhibited the best PL performance, attributed to their high crystallinity and plano-convex lens-like microstructure. In contrast, the nanowires exhibited worst PL performance due to the high density of surface defects, poor heat dissipation ability and poor light confinement, caused by the small diameters. This study not only achieved the controllable synthesis of various perovskite microstructures but also elucidated the relationships between morphology and optical properties. These findings provide a solid foundation for the broader application of perovskite materials in optoelectronic devices and related fields.

Declaration of Competing Interest

The authors declare that they have no known competing financial interests or personal relationships that could have appeared to influence the work reported in this paper.

Acknowledgments

This work was supported by the National Natural Science Foundation of China (Grant No. 11804025).

References

[1] Meiler, T.; Wang, Y.; Srivastava, S.; Adamo, G.; Paniagua-Dominguez, R.; Kuznetsov, A.; Soci, C. Wavelength Control of Perovskite Metasurface Lasing via Electrical Microheaters. Advanced Optical Materials 2023, 11 (10), 2202716. DOI: 10.1002/adom.202202716.

[2] Liu, Z.; Huang, S.; Du, J.; Wang, C.; Leng, Y. Advances in inorganic and hybrid perovskites for miniaturized lasers. Nanophotonics 2020, 9 (8), 2251-2272. DOI: 10.1515/nanoph-2019-0572.

ISSN: 2414-1895 DOI: 10.6919/ICJE.202505_11(5).0001

[3] Utzat, H.; Sun, W. W.; Kaplan, A. E. K.; Krieg, F.; Ginterseder, M.; Spokoyny, B.; Klein, N. D.; Shulenberger, K. E.; Perkinson, C. F.; Kovalenko, M. V.; Bawendi, M. G. Coherent single-photon emission from colloidal lead halide perovskite quantum dots. Science 2019, 363 (6431), 1068-+. DOI: 10.1126/science.aau7392.

[4] Chauhan, K. K.; Prodhan, S.; Ghosh, D.; Waghale, P.; Bhattacharyya, S.; Dutta, P. K.; Datta, P. K. Long Carrier Diffusion Length and Slow Hot Carrier Cooling in Thin Film Mixed Halide Perovskite. Ieee Journal of Photovoltaics 2020, 10 (3), 803-810. DOI: 10.1109/jphotov.2020.2976032.

[5] Wang, H.-C.; Lin, S.-Y.; Tang, A.-C.; Singh, B. P.; Tong, H.-C.; Chen, C.-Y.; Lee, Y.-C.; Tsai, T.-L.; Liu, R.-S. Mesoporous Silica Particles Integrated with All-Inorganic CsPbBr3 Perovskite Quantum-Dot Nanocomposites (MP-PQDs) with High Stability and Wide Color Gamut Used for Backlight Display. Angewandte Chemie International Edition 2016, 55 (28), 7924-7929. DOI: 10.1002/anie.201603698.

[6] Garnett, E. C.; Brongersma, M. L.; Cui, Y.; McGehee, M. D. Nanowire Solar Cells. Annual Review of Materials Research 2011, 41, 269-295. DOI: 10.1146/annurev-matsci-062910-100434.

[7] Li, J.; Xu, L.; Wang, T.; Song, J.; Chen, J.; Xue, J.; Dong, Y.; Cai, B.; Shan, Q.; Han, B.; Zeng, H. 50-Fold EQE Improvement up to 6.27% of Solution-Processed All-Inorganic Perovskite CsPbBr3 QLEDs via Surface Ligand Density Control. Advanced Materials 2017, 29 (5), 1603885. DOI: 10.1002/adma.201603885.

[8] Tian, J.; Tan, Q. Y.; Wang, Y.; Yang, Y.; Yuan, G.; Adamo, G.; Soci, C. Perovskite quantum dot topological laser. Nature Photonics 2024, 18 (2), 134-140. DOI: 10.1038/s41566-023-01234-7.

[9] Gao, Z.; Zhou, H.; Dong, K.; Wang, C.; Wei, J.; Li, Z.; Li, J.; Liu, Y.; Zhao, J.; Fang, G. Defect Passivation on Lead-Free CsSnI3 Perovskite Nanowires Enables High-Performance Photodetectors with Ultra-High Stability. Nano-Micro Letters 2022, 14, 215. DOI: 10.1007/s40820-022-00964-9.

[10] Cheng, H.; Ding, S.; Hao, M.; Wang, L.; Steele, J. A. Perovskite quantum dots: What's next? Next Energy 2024, 4, 100152. DOI: 10.1016/j.nxener.2024.100152.

[11] Li, X.; Aftab, S.; Mukhtar, M.; Kabir, F.; Khan, M. F.; Hegazy, H. H.; Akman, E. Exploring Nanoscale Perovskite Materials for Next-Generation Photodetectors: A Comprehensive Review and Future Directions. Nano-Micro Letters 2025, 17 (28). DOI: 10.1007/s40820-024-01501-6.

[12] Luo, P.; Zhou, S.; Xia, W.; Cheng, J.; Xu, C.; Lu, Y. Chemical Vapor Deposition of Perovskites for Photovoltaic Application. Advanced Materials Interfaces 2017, 4 (8), 1600970. DOI: 10.1002/admi.201600970.

[13] Wu, Z.; Chen, J.; Mi, Y.; Sui, X.; Zhang, S.; Du, W.; Wang, R.; Shi, J.; Wu, X.; Qiu, X.; et al. All-Inorganic CsPbBr3 Nanowire Based Plasmonic Lasers. Advanced Optical Materials 2018, 6 (18), 1800674. DOI: 10.1002/adom.201800674.

[14] Xu, W. L.; Niu, M. S.; Yang, X. Y.; Chen, H. Y.; Cai, X. H.; Smith, T. A.; Ghiggino, K. P.; Hao, X. T. Chemical vapor deposition growth of phase-selective inorganic lead halide perovskite films for sensitive photodetectors. Chinese Chemical Letters 2021, 32 (1), 489-492. DOI: 10.1016/j.cclet.2020.05.017.

[15] Hulbert, B. S.; Kriven, W. M. Specimen-displacement correction for powder X-ray diffraction in Debye–Scherrer geometry with a flat area detector. Journal of Applied Crystallography 2023, 56 (160–166). DOI: 10.1107/S1600576722011360.

[16] Holzer, V.; Schrode, B.; Simbrunner, J.; Hofer, S.; Barba, L.; Resel, R.; Werzer, O. Impact of sample misalignment on grazing incidence x-ray diffraction patterns and the resulting unit cell determination. Review of Scientific Instruments 2022, 93 (6), 063906. DOI: 10.1063/5.0088176.

[17] Zhao, D.; Zhang, C.; Zhang, X. X.; Cai, L.; Zhang, X.; Luan, P. S.; Zhang, Q.; Tu, M.; Wang, Y. C.; Zhou, W. Y.; et al. Substrate-induced effects on the optical properties of individual ZnO nanorods with different diameters. Nanoscale 2014, 6 (1), 483-491. DOI: 10.1039/c3nr04300b.

[18] Lao, X. Z.; Zhou, W.; Bao, Y. T.; Wang, X. R.; Yang, Z.; Wang, M. Q.; Xu, S. J. Photoluminescence signatures of thermal expansion, electron-phonon coupling and phase transitions in cesium lead bromide perovskite nanosheets. Nanoscale 2020, 12 (13), 7315-7320. DOI: 10.1039/d0nr00025f.

[19] Yu, B. Y.; Zhang, C. F.; Chen, L.; Huang, X. Y.; Qin, Z. Y.; Wang, X. Y.; Xiao, M. Exciton linewidth broadening induced by exciton-phonon interactions in CsPbBr₃ nanocrystals. Journal of Chemical Physics 2021, 154 (21). DOI: 10.1063/5.0051611.

ISSN: 2414-1895 DOI: 10.6919/ICJE.202505_11(5).0001

[20] Zhao, J.; Liu, M.; Fang, L.; Jiang, S.; Zhou, J.; Ding, H.; Huang, H.; Wen, W.; Luo, Z.; Zhang, Q.; et al. Great Disparity in Photoluminescence Quantum Yields of Colloidal CsPbBr3 Nanocrystals with Varied Shape: The Effect of Crystal Lattice Strain. The Journal of Physical Chemistry Letters 2017, 8 (12), 3115-3121. DOI: 10.1021/acs.jpclett.7b01083.

[21] Mahjabin, S.; Haque, M. M.; Sobayel, K.; Jamal, M. S.; Islam, M. A.; Selvanathan, V.; Assaifan, A. K.; Alharbi, H. F.; Sopian, K.; Amin, N.; Akhtaruzzaman, M. Perceiving of Defect Tolerance in Perovskite Absorber Layer for Efficient Perovskite Solar Cell. IEEE Access 2020, 8, 106346-106353. DOI: 10.1109/ACCESS.2020.3000217.

[22] Hong, D.; Zhang, Y.; Pan, S.; Liu, H.; Mao, W.; Zhang, W.; Ye, Y.; Wei, Z.; Lu, X.; Wang, X.; et al. Unveiling non-radiative center control in CsPbBr3 nanocrystals: A comprehensive comparative analysis of hot injection and ligand-assisted reprecipitation approaches. Nano Research 2024, 17 (5), 4525-4534. DOI: 10.1007/s12274-023-6326-2.

[23] An, R.; Zhang, F.; Zou, X.; Tang, Y.; Liang, M.; Oshchapovskyy, I.; Liu, Y.; Honarfar, A.; Zhong, Y.; Li, C.; et al. Photostability and Photodegradation Processes in Colloidal CsPbI3 Perovskite Quantum Dots. ACS Applied Materials & Interfaces 2018, 10 (44), 39222-39227. DOI: 10.1021/acsami.8b14480.

[24] Tian, F. S.; Yuan, C. X.; Chen, S. M. Influence of Light-Matter Interaction on Efficiency of Quantum-Dot Light-Emitting Diodes. Journal of Physical Chemistry Letters 2022, 13 (44), 10312-10317. DOI: 10.1021/acs.jpclett.2c02815.

[25] Xiao, L. B.; Xu, X. L.; Zhao, J.; Wang, C.; Lu, Z.; Li, L. T.; He, L.; Chen, Y.; Zou, G. F. High-Temperature Driven Recrystallization for Stable Dopant-Free α-FAPbI₃ Perovskite Solar Cells. Advanced Science 2024, 11 (48). DOI: 10.1002/advs.202408684.

[26] Tan, Q. L.; Zhao, J.; Li, Q. X.; Liu, H.; Dong, B.; He, C. G.; Chen, Z. T.; Zhou, W.; Liu, N. Y. Planar Compound Eye Lens for Enhanced Light Extraction Efficiency in AlGaN-Based Deep Ultraviolet LEDs. Advanced Photonics Research 2024, 5 (3). DOI: 10.1002/adpr.202300309.